Computational-based Aerodynamic Design for a Formula SAE Vehicle

Daniel Kelly, Jessica Batty, Thomas Carrel-Billiard, Anna Cybulsky and Lucien Viala
McGill Racing Team, McGill University, Montreal, Canada

Yvan Dumas, Nina Visconti and M'Hammed Mountassir
Quantisweb Technologies, Montreal, Canada

Abstract

The computational analysis and design of an aerodynamics system for a Formula SAE vehicle is presented. The work utilizes a stochastic-approximation optimization (SAO) process coupled with a computational fluid dynamics (CFD) solver. The methodology is presented in a general manner, and is applicable to other complex parametrizable systems. A mix of discrete and continuous variables is established to define the airfoil profile, location, sizing and angle of all wing elements. Objectives are established to maximize downforce, minimize drag and maintain a target vehicle aerodynamic balance. A combination of successive 2D and 3D CFD evaluations have achieved vehicle aerodynamic performance targets at a minimal computational cost.

Introduction

The Formula SAE competition challenges students to design and manufacture an open-wheeled race car for competition in a variety of static and dynamic evaluations. Here, the dynamic events of autocross and endurance feature an autocross-style course, governed by competition regulations to have short straights and tight corners [1].

While the competition regulations have always permitted aerodynamic devices, widespread presence of such devices has increased in recent years. A heuristic evaluation of the Formula Student Germany (FSG) competition reveals that each of the top five competitors in 2014 used aerodynamic devices [2]. This contrasts with 2006, where none of the FSG top five overall teams had aerodynamics [3]. This rapid growth has been partially due to advances in computational and experimental approaches. In the present state of the competition, a systematic development sequence is required to design a competitive aerodynamics system for the Formula SAE vehicle.

The conception of devices for aerodynamic downforce in the Formula SAE series is documented in the literature. For example, a recent study conducted at Loughborough University by Craig and Passmore [4] concluded that an aerodynamics package can result in a theoretical point gain at competition. Here, a thorough vehicle evaluation was performed, using a lap-time simulation tool, 2D Computational Fluid Dynamics (CFD), and model-size wind tunnel testing. Additionally, Wordley and Saunders [5] of Monash University evaluated aerodynamic devices on Formula SAE vehicles in 2006. Their approach experimentally investigated the track performance using multi-element wings in skid pad and autocross events, showing up to 30% improvements in cornering potential. These works demonstrate the potential performance gains attributed to aerodynamic devices.

In 2014, major revisions were made to the Formula SAE competition rules restricting the size and placement of aerodynamic devices [1]. Therefore, a complete re-evaluation of vehicle aerodynamics is required to remain rules-compliant and competitive in the 2015 season. To coordinate the numerous design selections and balance competing system objectives, a numerical optimization approach to aerodynamic design has been pursued. Due to the low-aspect ratio wings and highly three-dimensional airflow encountered on a Formula SAE vehicle, optimization on the entire vehicle in 3D is desired. To meet deadlines on a restricted design cycle, a high efficiency, rapid iteration process is required.

The use of a stochastic-approximation optimization (SAO) process [6] is proposed. This process is initialized by defining and prioritizing key parameters and design objectives. Then, a minimal Dynamic Design-of-Experiments (*m*DDOE) is generated, followed by the generation of the Result-of-Experiments (ROE) table. Next, a non-linear mathematical model is generated. Finally, optimization is performed on this model to generate the final design.

In the present work, the SAO methodology is implemented in the design cycle of a Formula SAE aerodynamics system. Here, primary objectives are to determine the sensitivity of overall vehicle aerodynamic performance to airfoil geometry, sizing and positioning of aerodynamic elements. Aerodynamic performance ROE tables are obtained via CFD computations, in communication with the SAO approach in loose-coupling.

First, the aerodynamic targets for the vehicle are derived, citing the assembly of a lap-time simulation model. The SAO process is then discussed, along with a description of the solvers used. A validation case for the CFD solver is provided. Successively, the baseline aerodynamic configuration for the vehicle is introduced. An initial analysis of the vehicle is performed via 2D aerodynamic analysis and SAO. Finally, the process is applied to full-vehicle 3D simulation. An ideal configuration and findings are discussed.

Background

The passage of air over a wing results in the generation of aerodynamic forces [7]. These forces resolve into two primary components: drag, which acts parallel to the airflow, and lift, which acts perpendicular to

the airflow. Figure 1 summarizes these forces on a two-dimensional wing cross-section:

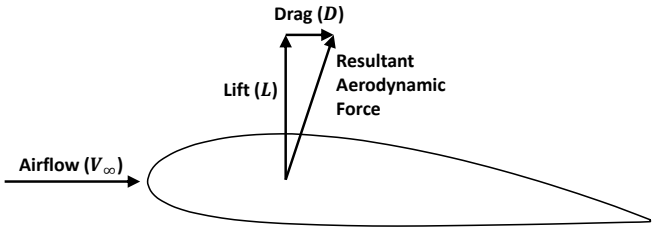

Figure 1: Aerodynamic forces on an airfoil

A non-dimensional expression for lift, the lift-coefficient, relates the lifting-properties of a body to air density, velocity and wing size:

$$C_L = \frac{L}{\frac{1}{2}\rho V^2 A} \quad (1)$$

Conversely, the non-dimensional term for drag, the drag coefficient, is defined as:

$$C_D = \frac{D}{\frac{1}{2}\rho V^2 A} \quad (2)$$

Aerodynamics and the Race Vehicle

Aerodynamic forces can have a significant impact on the performance of a race vehicle. When lift is directed towards the ground on a vehicle, hereinafter referred to as downforce, a greater effectiveness is achieved from the tires [8], thereby permitting corners to be travelled at a higher velocity and braking distances to be reduced. This corresponds to a potential reduction in lap times. Typically, downforce is generated through wings with inverted airfoil elements mounted at a negative angle of attack, shown in Figure 2.

On the racing vehicle, wings are frequently composed of multiple airfoil elements in a multi-element configuration featuring one or more flaps as per Figure 3. The multi-element configuration allows the race engineer to rapidly change the wing's lift and drag characteristics through a simple adjustment of the flap angle(s).

Figure 2: Rear wing on a race car

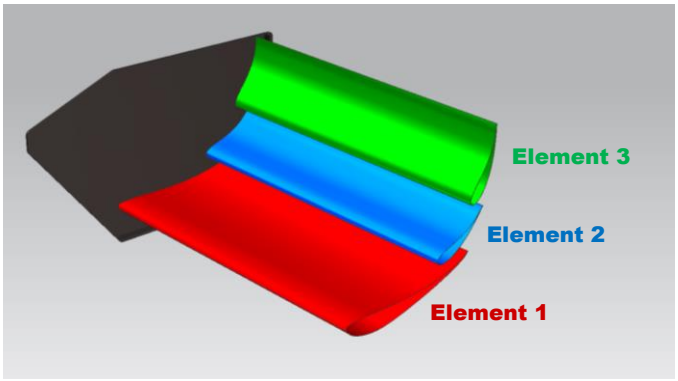

Figure 3: Multi-element wing configuration generating downforce

Methodology

The design of a high-performance multi-element aerodynamics package requires the placement of airfoils to achieve desired performance targets. Figure 4 proposes the implementation of an SAO process to drive CFD simulations. A series of decision variables, desired parametric limits and constraints are defined and prioritized with respect to the wing geometry, sizing and placement. The *m*DDOE provides an initial set of experimental wing geometries, in the form of a seemingly *traditional* Design-of-Experiments (DOE) table. For each aerodynamic configuration, the geometry is meshed and an evaluation is performed using a CFD solver. Aerodynamic results are tabulated, and returned as an ROE table.

The stochastic approximation mathematics algorithm processes the data, and generates behavioral laws to build the system's mathematical model. Considering the design targets, the decision variables and the constraints, a solution to the mathematical model is generated; this solution is referred to as the optimized parameter values (OPV). The OPV configuration is then evaluated using the CFD solver. If the performance of the OPV configuration does not meet the outputs from the CFD solver within a desired tolerance, the *m*DDOE table is populated with additional data points to improve the mathematical model. The process is repeated iteratively until convergence between the mathematical model and CFD solver are met. While the present work discusses aerodynamics on a race vehicle, the SAO process is general in its implementation, and may be applied to any complex system from which a model may be derived.

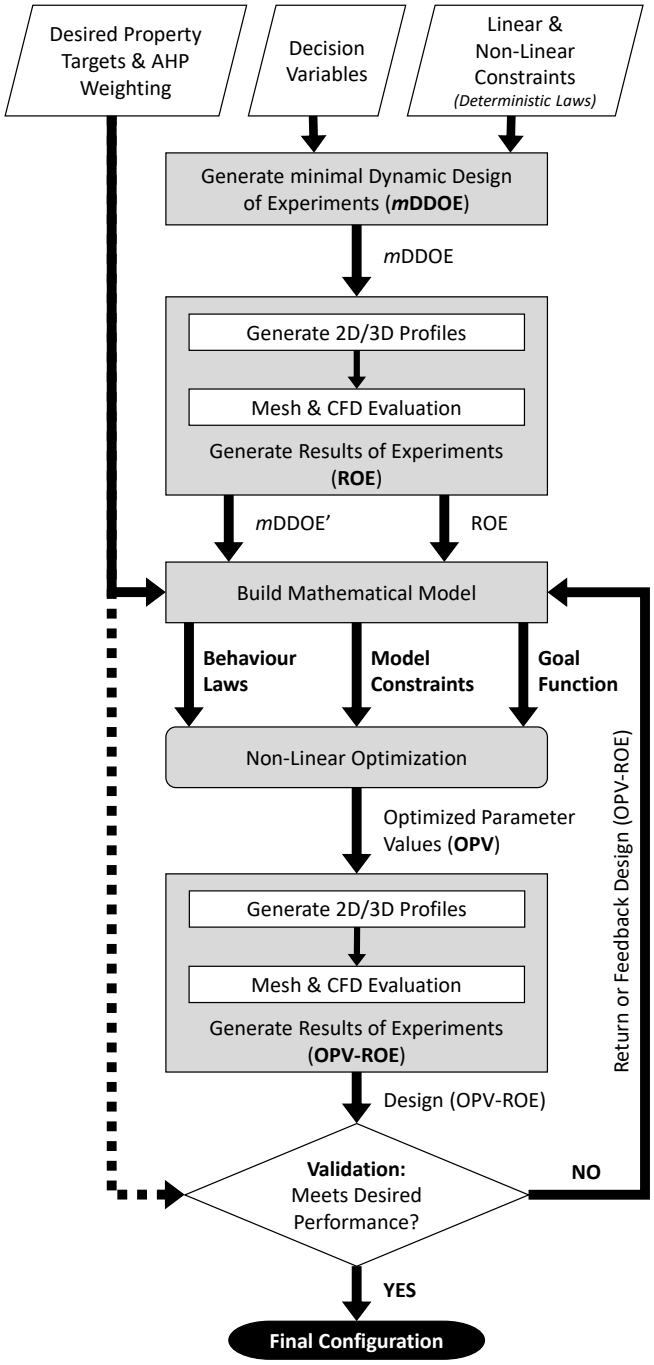

Figure 4: Framework for the stochastic-approximation optimization (SAO) process for aerodynamic systems

SAO software

The selected SAO process is the Quantisweb® methodology and software [6]. The process follows four main steps: first, a multi-criteria pair-wise comparison method orders desired properties according to their importance as defined by the user, based on the principles of the Analytic Hierarchy Process (AHP) [9]. The second step models the desired properties with an *m*DDOE through a library of statistical methods. In the third step, the model is generated based on actual experimental parametric values and output property variables extracted from the ROE.

The fourth step executes the non-linear optimization. A multifactorial and multidimensional goal function is generated primarily from the ideal target values and property weights, including properties, physical deterministic laws, and the information from the above mentioned three previous steps. The SAO process then references a library of hybrid optimization, which optimizes the goal function subject to the constraints represented by deterministic laws and stochastic-approximation laws (behavior laws). These laws can be linear, conditional, or non-linear (such as trigonometric functions). This methodology is applied iteratively to refine the final solution.

CFD Aerodynamic Solver

Aerodynamic properties are calculated using the CD-Adapco solver Star-CCM+ [10]. This code is a Navier-Stokes finite-volume 2D/3D CFD solver. The solver features Reynold's average Navier-Stokes (RANS) techniques for turbulence calculation. The code can analyze complex geometries via an internal CAD client and hexahedral-element mesh generation tools. Custom code has been written to employ these tools to rapidly setup geometry and meshing to this application.

CFD Validation

The performance of the CFD solver for airfoils in ground effect has been validated against wind-tunnel testing. Experimental work conducted by Zhang, et al [11], evaluated an inverted single-element wing in a belt-driven rolling road facility. In their work, a wing featuring a span of 1.100 m and a constant chord length of 0.2234 m was tested in a rolling-ground facility. The airfoil profile was a modified LS(1)-0413, referred to as the 'Tyrell 26' profile. Rectangular endplates were fitted to both ends. Pressure taps were installed spanwise and chordwise along the wing at several sections. A range of height-to-chord (h/c) ratios of 0.05 to 1.00 were tested at an incidence angle of 1 degree. Reynold's numbers of 2.98×10^5 and 4.47×10^5 were evaluated; these values are representative of a Formula SAE vehicle on an autocross course. Additional information on the experimental setup is available in the literature.

A 600,000 cell 3D mesh was generated over the Tyrrell 26 airfoil at an incidence angle of 1 degree; the mesh is illustrated in Figure 5. High y^+ wall treatment was applied to reduce computational cost, and a y^+ value of approximately 100 was calculated in the first structured layer. Steady CFD calculations were performed using the Realizable k-ε turbulence model with free transition. This model has been shown in the literature to be suitable for calculations on inverted wings in ground-effect [12, 13].

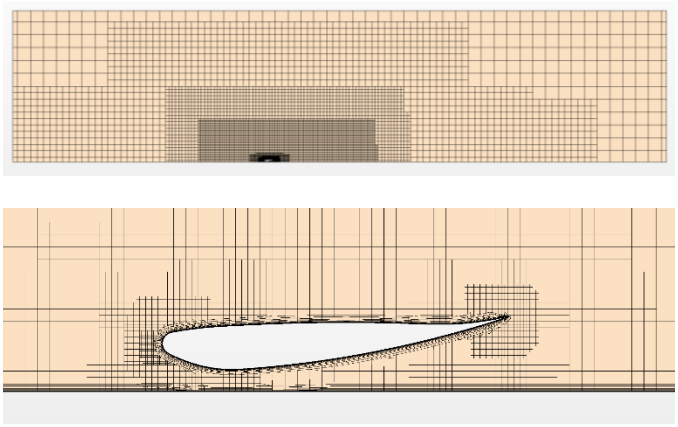

Figure 5: Illustrations of the Tyrrell 026 wing geometry and hexahedral mesh at h/c = 0.134

Figure 6 and Figure 7 summarize the computed aerodynamic values and experimental results from the literature. A comparison of pressure coefficient results at an h/c of 0.134 demonstrated good agreement near the center section of the wing (182 mm from the mid-span), and fair agreement near the tip (500 mm from the mid-span). A comparison of lift coefficient at varying ground clearances was shown to have good correspondence with experimental results for the free transition case. A peak lift coefficient within 3% of the experimental value was calculated by the CFD solver.

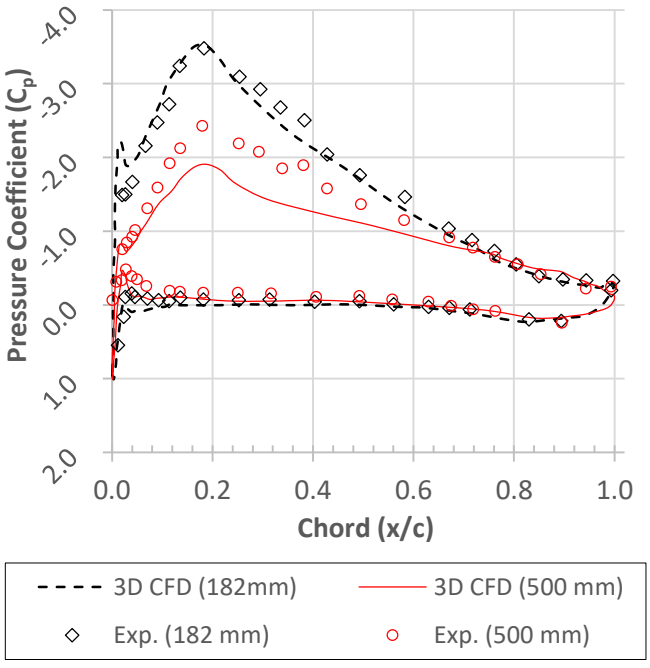

Figure 6: Plot of pressure coefficient on the Tyrrell 26 airfoil at h/c = 0.134

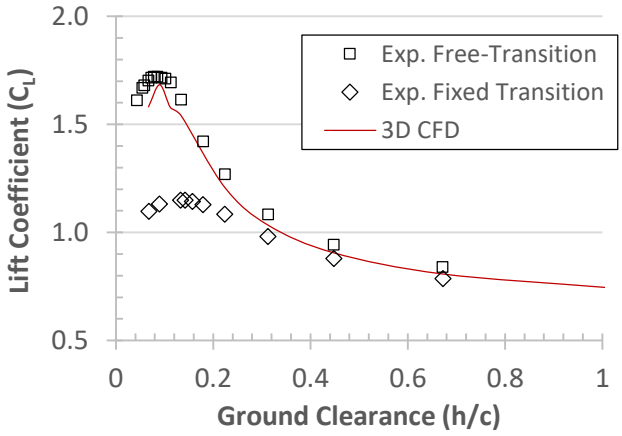

Figure 7: Tyrrell 26 Lift Coefficient at Varying Ground Clearance

Aerodynamic and Performance Targets

Balancing the competing effects of lift and drag is a significant factor in vehicle aerodynamics: while the increase in downforce allows for cornering with greater lateral acceleration and braking with higher deceleration, this comes at the cost of drag which negatively impacts acceleration and top speed. To assist in setting vehicle aerodynamic targets, the present work employs a lap-time simulation model deriving from work proposed by Patton [14]. This approach models the vehicle as a point mass on a track curvature profile. The velocity profile is developed from lateral grip capacity as well as acceleration and braking capabilities of the vehicle as collected from onboard data acquisition.

The 2014 FSG endurance course [15] is a good representation of a typical Formula SAE circuit; this course features tight corners and a maximum speed of around 25 ms^{-1}. A lap-time analysis for this course, in combination with a feasibility study, set the vehicle aerodynamic targets to a minimum lift coefficient of 4.0 and a maximum drag coefficient of 2.0 (with a reference area of 1 m^2). A parameter sensitivity analysis revealed that a larger focus should be placed on maximizing downforce generation than on minimizing drag reduction. An additional target was to achieve an aerodynamic balance within 5% wheelbase of the Centre of Gravity (CG) location.

Baseline Aerodynamic Configuration

The SAO non-linear optimization has the capability to adjust continuous and discrete variables to define a complex system. A priori, a baseline configuration and preliminary sizing of the aerodynamics system is required. The use of 2D and 3D CFD techniques in heuristic/trial-and-error methods established a baseline configuration which: a) met the physical limits of the regulations, and b) enabled enough flexibility to meet the desired aerodynamic targets. A three-device vehicle configuration was selected, featuring a front wing, a mid-region aerodynamic device, and a rear wing.

Significant consideration was given to selecting the configuration of each aerodynamic device, as a primary vehicle goal was to maintain an aerodynamic balance near the vehicle CG. To minimize airflow disruptions to the rear wing, a biplane configuration has been selected for the front wing. This wing features a two-element device below the nose cone and another two-element device above the nose.

The rear wing utilizes a three-element configuration featuring a main element and two flaps. A stand-alone fourth element has been added near the top of the main roll hoop to augment downforce. This rear wing design allows for a compromise between aerodynamic performance, adjustability, and manufacturability.

To compensate for the geometric restrictions on the front and rear wing, a focus was made on maximizing the downforce generated in the mid-region. In lieu of an undertray, a multi-element mid-region wing, installed alongside the driver compartment, has been selected. CFD analysis assisted in selecting a four-element design, featuring a lower main plane with two flaps, and a separate upper element.

The resulting aerodynamic configuration consisted of twelve wing elements on three aerodynamic devices, illustrated in Figure 8:

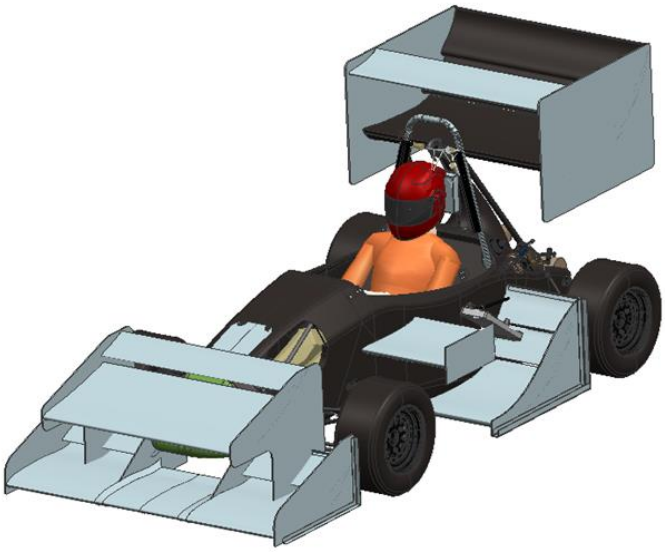

Figure 8: Aerodynamic Configuration for MRT16

Aerodynamic Optimization

Optimization commenced with the parameterization of aerodynamic devices via continuous and discrete variables. Fourty-six continuous variables were derived to define the chord length, relative position, geometric angle, overlap and gap spacing between elements on the full vehicle. The geometry of each element was further determined using discrete variable selection, from which the optimization solver could choose from a database of known airfoil geometries.

The use of discrete variables for airfoil selection results in a combinational problem with an exponential number of terms according to the following formula,

$$Possibilities = n^m \quad (3)$$

Where n is the number of airfoil geometries in the database and m is the number of element locations; in this case, 12 geometries and 12 wing element locations are employed. In combination with the numerous continuous variables to define the geometry, this created a very difficult mixed-integer non-linear optimization problem.

To minimize computational cost, the process was implemented in two phases. During phase 1, 2D CFD was performed on isolated aerodynamic devices: front wing, mid-region and rear wing. Phase 2 made use of 3D CFD, and incorporated the entire vehicle geometry to capture the complex aerodynamic interactions between the wings, wheels, ground and chassis. The strategic use of low-cost 2D CFD methods at early phases maximized the convergence rate towards desired performance targets within the limited timeframe. Design iterations were rapidly analyzed while considering mixed-integer/discrete variable problems, and effectively the total number of possible configurations was reduced.

Phase 1: 2D Aerodynamic Process

The primary deliverable of Phase 1 was to establish the local wing interaction effects within each aerodynamic device (front wing, mid-region and rear wing). Each airfoil geometry was set via discrete variable optimization. Parameter limits were also refined in preparation for 3D CFD.

Modeling and Setup

Decision variables and respective parametric limits defining the relative positioning between wing elements for each aerodynamic device were determined. A summary of a parameterized mid-region wing section is demonstrated by Table 1 and Figure 9. Some of the constraints and parameter limits were set based on geometric / rules restrictions; the remaining parameter limits were set based on multi-element aerodynamic theory [16, 17].

Table 1: Decision variables for the aerodynamic optimization process

Name	Description	Variable Type
XL	x-coordinate lower element	Continuous
YL	y-coordinate lower element	Continuous
XU	x-coordinate upper element	Continuous
YU	y-coordinate upper element	Continuous
C1	Chord length lower main	Continuous
C2	Chord length lower flap 1	Continuous
C3	Chord length lower flap 2	Continuous
C4	Chord length upper main	Continuous
A1	Angle of attack lower main	Continuous
A2	Angle of attack lower flap 1	Continuous
A3	Angle of attack lower flap 2	Continuous
A4	Angle of attack upper main	Continuous
G1	Elements 1-2 gap spacing	Continuous
G2	Elements 2-3 gap spacing	Continuous
O1	Elements 1-2 overlap	Continuous
O2	Elements 2-3 overlap	Continuous
AF1	Airfoil 1 Geometry	Discrete
AF2	Airfoil 2 Geometry	Discrete
AF3	Airfoil 3 Geometry	Discrete
AF4	Airfoil 4 Geometry	Discrete

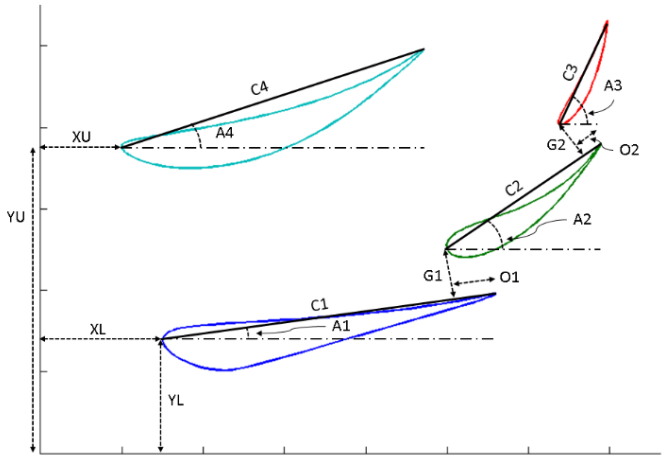

Figure 9: Sample aerodynamic configuration for the mid-region aerodynamic device

High-lift airfoil geometries were selected from the literature to maximize aerodynamic downforce potential; a total of 12 airfoils with a $c_{l_{max}}$ exceeding 1.5 were selected. Considerations were made to incorporate variability in airfoil geometries, as to select profiles deemed suitable as main plane, flap, and/or isolated wing elements. This controlled selection of airfoils allowed the team to omit geometries which could not easily be produced using available manufacturing methods. A library was populated containing airfoil element coordinates, and an integer value applied to each airfoil; the non-linear optimization solver could select the geometry of each element via discrete variable selection.

A code was written to generate geometry files based on input variables from the *m*DDOE table. Furthermore, 2D mesh generation and simulation setup was automated through custom macro tools. 2D CFD meshes of approximately 15,000 elements were generated for each geometry using polyhedral elements. A structured prism layer was featured around airfoil elements. Steady simulations were conducted at a freestream velocity of 20 ms^{-1}. The *Realizable k-ε* turbulence model was used, and a moving ground was considered for all simulations. Convergence of continuity residual was set to four orders of magnitude, ensuring a stabilization of c_d within 0.0001.

Primary optimization objectives were set to minimize drag and maximize downforce. A scaled weighting was applied to all objectives based on the lap simulation results, with a higher weighting applied to parameters having a greater influence on lap times. Outputs from the CFD solver were compiled into a matrix, and fed to the non-linear optimization solver to generate an OPV configuration. This configuration was evaluated through CFD. For Phase 1 evaluation, a convergence target of 5% between OPV desired values and CFD results was set. Successive runs to further populate the *m*DDOE table were performed until this convergence target was met.

To minimize the model complexity and computational expense, a progressive approach to airfoil selection was applied. In this strategy, the non-linear optimization solver had the ability to adjust the airfoil geometry featured on the first element while the geometry of the remaining elements was held constant. After the geometry of the first element was selected, the process was repeated for the remaining flap elements in sequence. Continuous decision variables were not restricted in this process. After selecting all airfoil geometries, further rounds of optimization were performed to determine the approximate element positioning.

Results

Several iterative rounds were required to reach a converged OPV configuration. The following table outlines the number of rounds and separate runs required to reach a converged OPV configuration.

Table 2: Phase 1 Aerodynamic Run Summary

Aerodynamic Device	OPV Rounds	Total Runs	Solution Discrepancy	
			Lift	Drag
Front Wing	11	403	2.2%	2.3%
Mid-Region	7	414	3.9%	1.2%
Rear Wing	12	755	3.2%	12.4%

Each aerodynamic device required over 400 runs and numerous *m*DDOE cycles to reach convergence between CFD and SAO solvers. This convergence target was achieved for lift coefficient; some discrepancies were noted in reaching convergence for drag coefficient on the rear wing. As this was a preliminary evaluation round and drag was not the primary optimization target, a decision was made to move forward to Phase 2 with the results obtained.

The absolute values of the aerodynamic coefficients obtained from 2D CFD were not thoroughly investigated; due to the three-dimensional effects of low aspect-ratio wings and the vehicle interactions, the 2D results were not indicative of overall vehicle performance. Instead, the quality of the CFD solutions and local wing interaction effects were analyzed to ensure the airfoil elements and resulting OPV configurations were valid. This was conducted through visual analysis of velocity contours and pressure coefficient plots. A sample pressure contour plot for the front wing is illustrated in Figure 10:

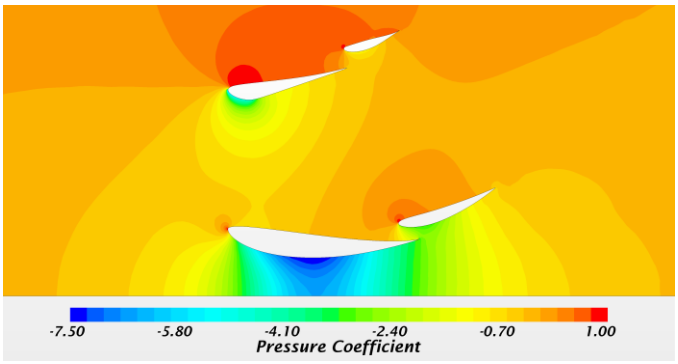

Figure 10: Front wing pressure coefficient contour plot from 2D sequence

The 2D CFD evaluation revealed important properties of the system's aerodynamic parameters and the loose-coupling methodology. The interaction between airfoils was found to be important, but in many cases several airfoils demonstrated potential as a good candidate for a given wing element (main plane, flap or isolated element). In some cases, the performance change between several airfoils yielded marginal (less than 1%) performance changes in the system. These findings suggest that within a small margin, airfoil selection is important, but the use of a multi-element configuration enables enough flexibility in the system to reach comparable performance values by varying element sizing and relative element position.

The results from the 2D analysis helped refine and adjust the parameter ranges ahead of the 3D optimization phase. For example, the parameter ranges for second flap elements on the mid-region and rear wing were adjusted to permit higher angles since the 2D optimizer placed these elements near their upper angle limits.

Phase 2: 3D Aerodynamic Process

The second phase coupled the SAO analysis with 3D Navier-Stokes calculations. A full-scale vehicle model, featuring the primary vehicle components, wheels, and all three aerodynamic devices, was employed. The airfoil geometries obtained through the Phase 1 analysis were retained; only continuous variables defining chord length and airfoil position were defined in Phase 2.

Modeling and Setup

Wing element position was defined in 3D via 46 continuous variables. Each wing element was modeled as a straight extrusion perpendicular to the vehicle centerline. Thirty-four constraints ensured conformity with the competition regulations [1] and geometric restrictions of the vehicle. Straight-line aerodynamic performance was evaluated using a half-body chassis model to reduce computational cost. The chassis model featured the monocoque and roll hoops, a driver, engine intake, wheels and suspension links. A custom macro constructed the wing geometry in a CAD client for each individual configuration. Generic endplates of 6mm thickness were added to all wings. Modifications to the chassis, including changes to ride height and pitch, were not considered. An illustration of the CFD geometry and mesh is included in Figure 11.

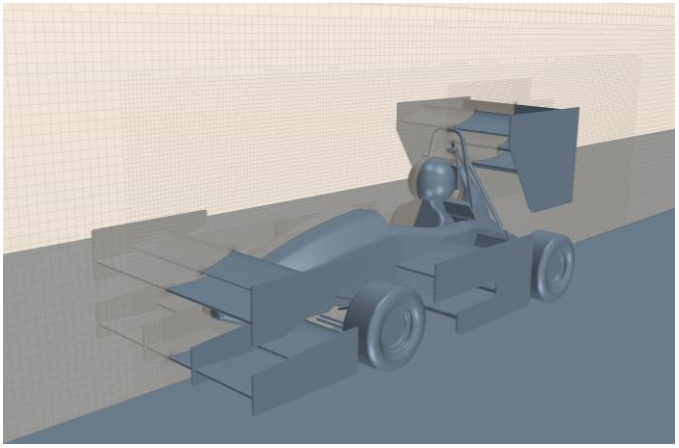

Figure 11: Illustration of the CAD/mesh geometry for the MRT16 vehicle

Hexahedral meshes of approximately 6 million cells were generated for each aerodynamic configuration. Prismatic refinement at the vehicle surface was used. Steady CFD calculations were made using the *Realizable k-ε* turbulence model. High y^+ wall treatment was applied to reduce mesh size and overall computational cost of the optimization process; an average wall y^+ value of 60 was observed. A moving ground was employed, and rotating wheels were modeled assuming zero slip. A uniform inflow velocity of 20 ms^{-1} was used, and Dirichlet boundary conditions were established at the outlet.

Unequal-weighting was applied to the optimization targets, which included maximum downforce, minimum drag, and vehicle center-of-pressure (CP) location (to set aerodynamic balance). Communication between the CFD and SAO was accomplished through *m*DDOE / aerodynamic result tables. A convergence target between the CFD and SAO model of 2% was set.

Results

CFD simulations were performed on 32 processors, reaching a converged solution in approximately 4 hours per run. A total of seven OPV cycles were performed, with additional CFD runs added to the DDOE table at each cycle. A total of 313 individual 3D CFD runs were required to obtain convergence between the SAO solver and CFD results, as summarized in Table 3.

Table 3: Phase 2 Aerodynamic Run Summary

OPV Rounds	Total Runs	Solution Discrepancy		
		Lift	Drag	CP Location
7	313	1.1%	0.4%	0.3%

The optimized configuration from the final model achieved a maximum in vehicle downforce at a drag coefficient of 1.6 and center of pressure location within 1% of the CG. These results were well within the desired performance targets.

In addition to an optimized aerodynamic configuration, the SAO process allows the user to acquire a perspective on the sensitivity of each parameter on the global aerodynamic system performance. For example, the front wing lower flap element angle was found to have the largest effect on vehicle balance; adjusting the angle from the minimum to the maximum parameter range caused a 13.5% change in CP location. However, changes in overall vehicle downforce due to front wing lower flap angles were less than 1% over the same parameter range. This identified the front wing flap as an ideal device to achieve balance adjustments without compromising overall aerodynamic performance. Such a model has immense capabilities when applied directly to vehicle testing, allowing a rapid estimation of the impact of configuration changes on vehicle performance.

Discussion

Using High Performance Computing (HPC) resources, solving large-scale 3D CFD problems has become more viable in recent years. The use of a SAO process, methodology and software permitted several benefits for the optimization of an aerodynamic system when CFD calculations were performed using HPC resources. This approach permitted the generation and validation of the mathematical model immediately after the first SAO cycle. One benefit of this iterative process was to allow numerous trials at the same time in a batch-oriented way, greatly accelerating the convergence towards an ideal configuration; within a four week design cycle, the use of batch-oriented CFD runs on an HPC cluster maximized the number of configurations evaluated. The large amount of collected data permitted improvements in the robustness of the model, and allowed for a better performance in the final aerodynamic configuration.

As many variables were modeled, the SAO approach provided a robust framework for identifying and understanding the trends of both small and large parameter changes (e.g. the influence of a flap angle change on aerodynamic coefficients). Furthermore, the inclusion of all aerodynamic variables across all aerodynamic devices in the same mathematical model ensured that the system's potential was well harnessed. As the optimization solver relied on mathematical models,

this process permitted the exploration of certain configurations that may not have been considered due to human biases.

The SAO process allows the user to acquire a large amount of information as to the sensitivity of each variable and its respective parameter value, as well as its potential for meeting design targets. The process of design validation through OPV assists the user in identifying all types of constraints. This allows for the refinement of the design, a critical step to reaching the chosen design targets. An increased understanding of the parametric interrelationship of the aerodynamics system and the magnitude of effects on the desired properties has been demonstrated through this present study.

The present approach affords a high level of flexibility and the ability to adapt to the needs of the process and the product. In this evaluation, 46 geometric variables and 12 airfoil geometries were considered for their impact on downforce and drag. As with all numerical techniques, the approach used in this work has some limitations. The approach is highly dependent on the quality of the parametrization of the initial problem. Solutions outside of the defined parameter ranges will not be explored; thus a high level of user experience is required in defining the parameters and bounds of the aerodynamic problem. The geometries used for this work were existing airfoil cross-section geometries, extruded with constant geometry across the wing's span. More complex configurations could have been evaluated, but would have increased the user input time required for implementation and modeling, as the number of parameters in the optimization problem would likely increase. Additional parameters would also increase the computational cost due to the increased number of ROE solutions required to obtain a robust mathematical model. For this work, the complexity level was chosen in consideration with the available computational resources and timeline restrictions.

Future work seeks to include the engine cooling radiators which mount between the lower and upper aerodynamic features in the mid-region on either side of the vehicle. The effects of the radiator system, in terms of aerodynamic and heat transfer effects, could be evaluated as parameters within the aerodynamic optimization process.

Summary/Conclusions

A system-level design process has been achieved to assist in the design of an aerodynamics system for a Formula SAE vehicle. The problem was large-scale and intractable, with requirements to meet design, time and regulatory constraints. Through this process, the following was achieved:

- A coupling of 2D and 3D CFD approaches with a stochastic-approximation optimization (SAO) process was successfully implemented
- An aerodynamic configuration consisting of 12 wing elements was selected as a baseline vehicle configuration for optimization
- 46 variables and 34 constraints were selected to define wing element position, chord length and geometric angle
- Each element's airfoil geometry was selected from a library of 12 through the SAO process coupled with 2D CFD
- An ideal aerodynamic configuration was reached using 3D CFD coupled with the SAO process, attaining maximum downforce at a drag coefficient of 1.6
- The communication between these two *cybernetic* systems, CFD and SAO, allowed for a faster and more efficient experimental design and likely a more cost effective route to a new product.

References

1. SAE International, "2015 Formula SAE Rules." http://students.sae.org/cds/formulaseries/rules/2015-16_fsae_rules.pdf, accessed Sept. 2015
2. Formula Student Germany, "FSC14 Overall Scoring Results." https://www.formulastudent.de/fsc/2014/results/, accessed Aug. 2015
3. Formula Student Germany, "Formula Student Germany: Overall Results." https://www.formulastudent.de/fsc/2006/results/#c415, accessed Aug. 2015
4. Craig, C. and Passmore, M., "Methodology for the Design of an Aerodynamic Package for a Formula SAE Vehicle," *SAE Int. J. Passeng. Cars - Mech. Syst.* 7(2):575-585, 2014, doi:10.4271/2014-01-0596.
5. Wordley, S. and Saunders, J., "Aerodynamics for Formula SAE: A Numerical, Wind Tunnel and On-Track Study," SAE Technical Paper 2006-01-0808, 2006, doi:10.4271/2006-01-0808.
6. Mountassir, M. "Method of optimizing parameter values in a process of producing a product," Canada Patent CA2382523 A1. Mar 15, 2001.
7. Abbott, I., and von Doenhoff, A., "Theory of Wing Sections." (Mineola, Dover Publications, 1959), ISBN 0486605868
8. McBeath, S., "Competition Car Aerodynamics: A Practical Handbook, 2nd Edition," (Somerset, Haynes Publishing, 2011), ISBN 0857330071
9. Saaty, T., "Fundamentals of the Analytic Hierarchy Process," (Pittsburgh, RWS Publications, 1996), doi:10.1007/978-94-015-9799-9_2
10. CD-Adapco. "STAR-CCM+user guide, Version 9.06," 2014.
11. Zerihan, J., and Zhang, X., "Aerodynamics of a Single Element Wing in Ground Effect." *Journal of Aircraft* 37(6): 1058-1064, 2000, doi:10.2514/2.2711
12. Barber, T., Doig, G., Beves, C., Watson, I. et al, "Synergistic integration of computational fluid dynamics and experimental fluid dynamics for ground effect aerodynamics studies." *J. Aerospace Engineering* 226(G): 602-619, 2012, doi: 10.1177/0954410011414321
13. Genua, E., "A CFD Investigation into Ground Effect Aerodynamics," Master's Thesis, Department of Aerospace Design, Integration and Operations, Delft University of Technology, Delft, 2009.
14. Patton, C., "Development of Vehicle Dynamics Tools for Motorsport," Ph.D. Dissertation, Mechanical Engineering Department, Oregon State University, Corvallis, 2013.
15. Formula Student Germany, "Formula Student Germany Event Handbook 2014, vol. 1.1," Hockenheim, 2014.
16. McBeath, S., "Wings," Competition Car Aerodynamics: 86-137, 2012
17. Smith, A. M. O., "High-Lift Aerodynamics." *Journal of Aircraft* 12 (6): 501-530, 1975, doi:10.2514/3.59830

Contact Information

Daniel A. Kelly
McGill Racing Team, McGill University, Montreal, Canada
daniel.kelly2@mail.mcgill.ca

Acknowledgments

Computations were made on the supercomputer Guillimin from McGill University, managed by Calcul Québec and Compute Canada. The operation of this supercomputer is funded by the Canada Foundation for Innovation (CFI), NanoQuébec, RMGA and the Fonds de Recherche du Québec - Nature et technologies (FRQ-NT).

Definitions/Abbreviations

A	reference area (m^2)
c	wing chord (m)
C_D	wing / body drag coefficient
C_L	wing / body lift coefficient
C_{Lmax}	maximum lift coefficient
CP	centre of pressure location
D	wing / body drag (N)
h	ground clearance height (m)
L	wing / body lift (N)
V	air velocity (m/s)
ρ	air density (kg/m^3)